Low-Mass RF Power Inverter for CubeSat Applications Using 3-D Printed Inductors

Wei Liang, *Student Member, IEEE*, Luke Raymond, *Student Member, IEEE*, Max Praglin, *Student Member, IEEE*, David Biggs, Fabio Righetti, Mark Cappelli, Brian Holman, and Juan Rivas Davila, *Member, IEEE*

***Abstract*— This paper presents the design of a low-mass RF power inverter at moderate to high power levels (e.g., tens of watts and above) for weight critical applications such as CubeSat plasma thrusters. Our approach for mass reduction includes resonant switching operation at tens of MHz, and the 3-D printing of lightweight scaffolds that form air core inductors after plating with a thin layer of copper. Specifically, we present a 14.2-MHz 50-W resonant dc-RF power inverter implemented with 3-D printed and copper plated air core toroidal inductors. As a demonstration of design flexibility of the 3-D printing process, these toroidal inductors are designed and implemented with optimal cross sections [1] to improve quality factors. The weight of the proposed inverter is reduced by 50% when compared to a 40-W state-of-the-art counterpart in which all the inductors were implemented within the printed circuit board. The inverter achieves 91% electrical efficiency when operated on a 50-Ω resistive load at an input voltage of 50 V. To prove its capability of driving plasma loads, the inverter was first tested with a matching network running an inductively coupled plasma (ICP) in a low-pressure argon ampoule outside vacuum environment. The inverter drew 50 W to run the ICP at an input voltage of 20 V. Then as an example application, the inverter was tested with another specifically tuned matching network to drive a helicon double layer (HDL) plasma intended for CubeSat thruster applications. The HDL plasma was formed in a vacuum chamber and was fed with argon. The combined inverter and matching network outputs 40 W and achieves 86% dc input to plasma efficiency at an input voltage of 40 V .**

***Index Terms*— CubeSat, RF power inverter, 3-D printed air core inductors.**

I. Introduction

CUBESATS, a subclass of microsatellites, consist of standardized components that take the form of one or multiple 10 cm cubes (or 1U). The recent popularity of the CubeSat platform is in part due to the low operation and launch costs that are putting "access to space" within the reach of academic institutions, small companies, and even individuals. There has also been interest in developing commercial applications using CubeSats, including imaging and monitoring of resources, communication, asteroid mining, etc. CubeSats are sometimes released into orbit from the international space station (ISS) [2] and can be deployed from rockets as secondary payloads as the rocket ascends to fulfill its primary mission. The Cubesats deployed from the ISS have a lifetime of just a few months as they travel in a decaying low earth orbit affected by atmospheric drag. Other CubeSats deployed from higher altitude rockets can last in space for years, but are often placed in noncircular or highly elliptic orbits that are suboptimal for imaging tasks. Hence, there is an increasing need for CubeSats to have microthruster systems for orbital maneuvering or station keeping.

Electric propulsion is a promising solution that has proven effective on large satellites and if miniaturized can be a significant asset to CubeSats. However, to date, electric propulsion is not a subsystem commonly available in CubeSats due to difficulties associated with scaling thruster systems down to a suitable size. Different types of electric propulsion systems used in large satellites, including Hall effect thrusters [3], [4], ion thrusters [5], helicon double layer (HDL) thrusters [6]–[8], and electrothermal plasma thrusters [9], are currently being evaluated for CubeSats. However, the power electronics appear to be a significant barrier for the practical deployment of these systems, considering the large size and weight of conventional power supplies.

Interest in smaller, lighter, and cheaper power electronics has never been greater for CubeSats. Although most power supplies are optimized for volume power density [10], applications such as power supplies for satellites and other space related applications benefit from even the smallest improvements in weight power density. As magnetics (inductors and transformers) are usually responsible for a large portion of the volume and weight, many studies propose different ways (wire wound [11], printed circuit board (PCB) [12], and nanofabrication [13]) to design and implement air core inductors for their advantages when used at high frequencies (no core losses, and no saturation or Curie temperature). In this paper, we present a dc-RF power supply design that achieves substantial improvements in weight power density and has the potential to enable the use of miniature plasma thrusters for CubeSats and other small spacecraft. Specifically, this paper proposes the 3-D printing of a lightweight scaffold that after plating with a thin layer of copper forms air core inductors for use in a high frequency resonant inverter. This approach reduces the weight of the converter by 50% compared with a similar design implemented with PCB-based inductors.

Manuscript received August 12, 2016; revised November 16, 2016; accepted December 11, 2016. Date of publication December 23, 2016; date of current version May 1, 2017. This work was supported by the Stanford University Precourt Institute of Energy. This work appeared in part at the 2016 *IEEE Workshop on Control and Modeling for Power Electronics,* Trondheim, Norway, 2016. Recommended for publication by Associate Editor F. J. Azcondo.

The authors are with Stanford University, Stanford, CA 94305 USA (e-mail: liangw@stanford.edu).

Color versions of one or more of the figures in this paper are available online at http://ieeexplore.ieee.org.

Digital Object Identifier 10.1109/JESTPE.2016.2644644

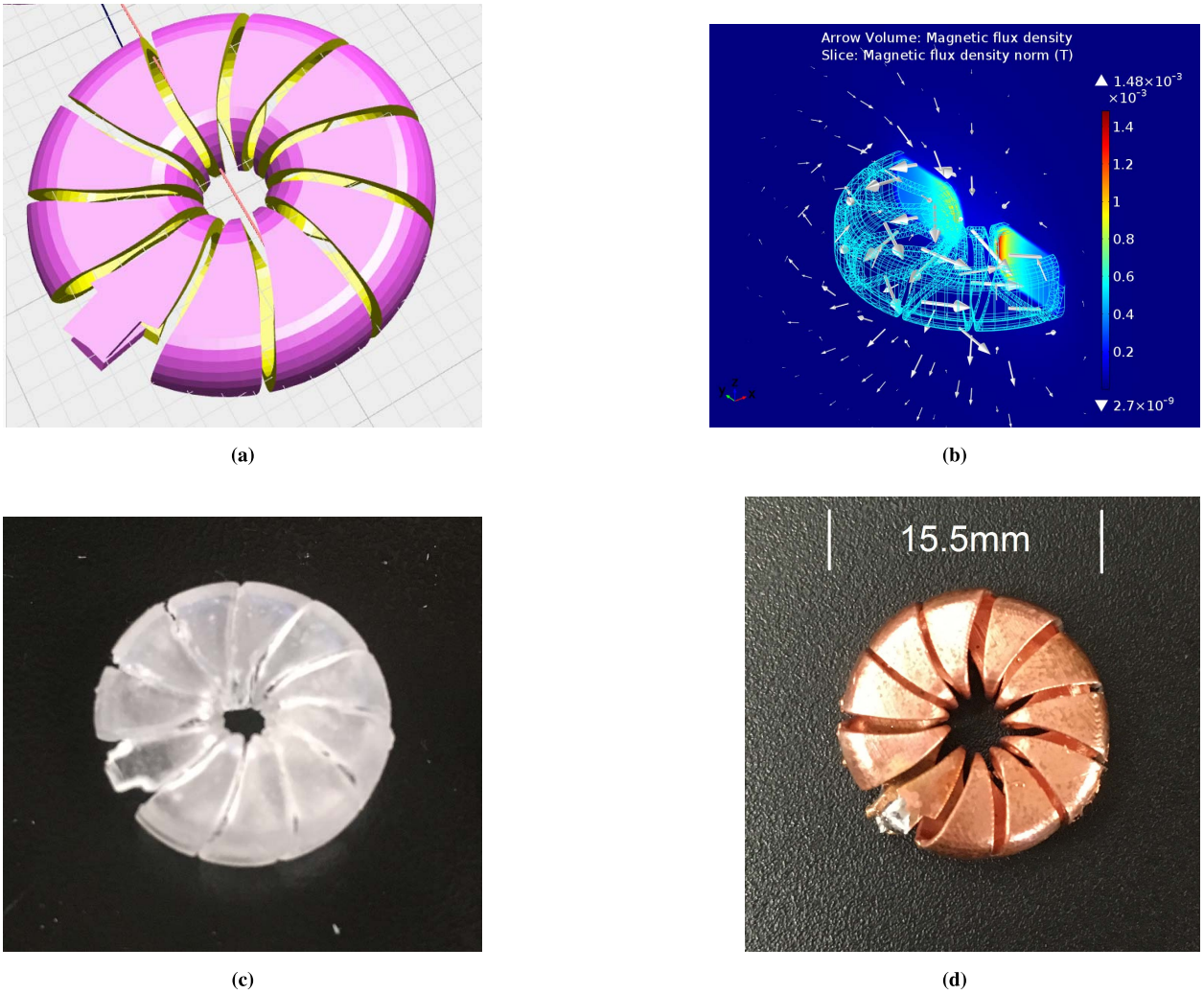

Fig. 1. Design and manufacturing process of the 3-D printed air core inductor. The specs are listed in Table I. (a) CAD model. (b) Flux density FEA from COMSOL Multiphysics. (c) 3-D printed plastic scaffold. (d) Plated scaffold with 50 μm of copper with an inductance of 90 nH.

This paper is outlined as follows. Section II presents the fabrication and characterization of the 3-D printed air core inductors. Experimental implementation and results of the proposed inverter prototype are presented in Section III. Sections IV and V present the experiments of the inverter driving an inductively coupled plasma (ICP) and an HDL plasma thruster. Section VI draws conclusions.

II. Low-Mass 3-D Printed Inductors

As demonstrated in [14], 3-D printing can increase design flexibility of air core inductors leading to higher quality factors (Q) and reduced electromagnetic interference. In [14], the inductor was first 3-D printed in a wax-like castable material and then lost-wax casting techniques were used to make the part a solid silver piece. However, the electrical conductivity of the silver used by the lost-wax casting service company (Shapeways, i.materialize) was lower than the nominal conductivity values of silver, possibly due to the chemical additives and impurity introduced during the casting process. Therefore, the measured quality factors of the silver inductors in [14] differed significantly from simulation. Moreover, because most of the inductors carry high-frequency ac currents, only a thin surface layer of the solid metal is utilized due to a skin depth of tens of μm.

An alternative to casting is to plate a thin layer (e.g., 50 μm) of metal directly onto the 3-D printed nonconductive scaffold. This can result in a significant weight and cost reduction without sacrificing performance or changing the field distribution within the magnetic structure. Therefore, the core manufacturing process of the inductors presented in this paper is similar to [14], but replaces casting with copper plating.

Fig. 1(a)–(d) shows the 3-D CAD model of one of air core inductors in our design, the 3-D printed plastic scaffold, the corresponding finite element analysis (FEA) simulation via COMSOL Multiphysics, and the finished copper plated inductor, respectively. This inductor was designed in OpenJSCAD, an online 3-D CAD scriptable modeling tool. A nonconductive plastic scaffold of the designed shape was 3-D printed in a low-cost Formlabs Form 1+ desktop stereolithographic printer. The 50-μm-thick copper plating on the plastic scaffold was outsourced to a commercial plating service (RePliForm, Inc.). The reason for choosing 50 μm plating thickness was the

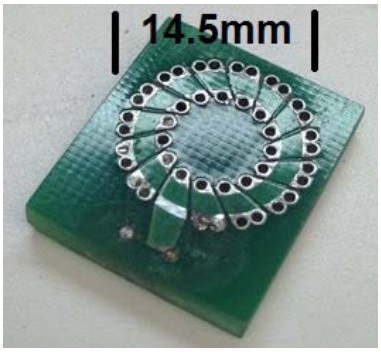

Fig. 2. 3.2-mm-thick 1-oz copper 81-nH PCB inductor (specs listed in Table I).

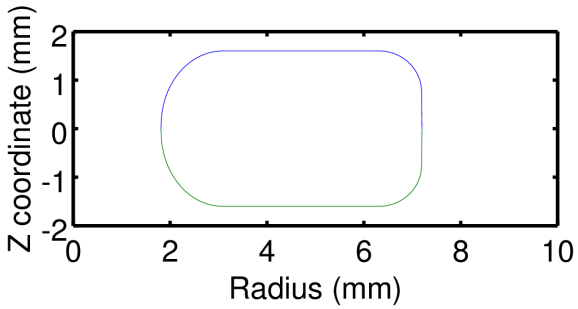

Fig. 3. Inner surface cross section of the inductor shown in Fig. 1(d) optimized using the script described in [1].

TABLE I
SPECIFICATIONS AND COMPARISON OF INDUCTORS IN FIGS. 1(d) AND 2. MEASUREMENTS ARE PERFORMED AT 27.12 MHz

Part	**OD/ID/ht/turns** [mm]	**L** [nH]	**Q**$_{MEAS}$
Fig. 1d	15.5/3/3.2/11	90 (98 in sims)	94 (105 in sims)
Fig. 2	14.5/8/3.2/15	81	80

result of a tradeoff between our goals of minimizing weight and ensuring that the plastic scaffold was fully plated. To minimize weight, we want the thinnest plating possible but greater than at least one skin depth at the operating frequency. At 14 MHz, the skin depth in copper is approximately 17 μm and thus sets the lower limit for plating thickness. Moreover, the majority of the magnetic flux is contained within the torus, which results in current crowding in the inner side of the toroid wall. So, having greater than skin depth plating thickness is necessary to achieve good quality factors. On the other hand, note that the minimum plating thickness and finishing quality achieved in practice depend heavily on the process capabilities of the plating house. Replifrom has not shared the specifications of their plating process, so we had to go through a trial-and-error phase, in which we ordered various inductors samples plated. The parts that were ordered with 50μm from Repliform came with consistent plating results. We have evaluated other plating houses, for example, ProtoLabs, that delivered a plating result of better visual quality at a much higher cost (>$200 USD per inductor versus $30 USD range from Repliform). Because the plating needs to be thicker than the skin depth to ensure sufficient current conduction (good quality factor), we chose Repliform in the current prototyping phase. As we get closer to realistic testing, and when designing a CubeSat payload, we will be inclined to have a better quality plating if the resources are available.

As a demonstration of the flexibility of 3-D printed magnetic structures, the inductor in Fig. 1(d) was designed to have an optimized cross section to minimize loss under specific outer diameter and height constraints. The design goal of the 3-D inductor in Fig. 1(d) is to be comparable (inductance and volume) to the PCB counterpart in Fig. 2, as well as achieving good balance in quality factor and weight reduction. This was done so that we could evaluate and compare two different methods of fabricating air core inductors. For a fair comparison, we aimed to design components with the same outer dimensions (outer diameter and height, which determine the volume) of the torus, and inductance as the PCB inductor. With the outer dimensions constrained, the inner diameter and the outline of the inductor inner surface cross section were obtained using the optimization script tool described in [1] and shown in Fig. 3. The fabricated 3-D inductor in Fig. 1(d) was then characterized using Agilent E5061B network analyzer for its frequency-dependent impedance and quality factor. Plots are shown in Fig. 4 at the frequency range of interest (10–50 MHz).

To evaluate the performance of the 3-D printed inductor with other air core inductor fabrication methods, the PCB inductors were chosen as the counterpart, because they have better copper usage per unit mass than the wire-wound ones due to skin effect. While achieving exact optimized cross-sectional shapes can be difficult in conventional toroidal air core inductor implementations (wire wound [11], PCB [12], and nanofabrication [13]), it is easily realized in the proposed 3-D printing and plating approach by using a simple CAD script in OpenJSCAD. Table I lists a performance comparison between the proposed design and its PCB counterpart shown in Fig. 2. The comparison shows that the 3-D printed and plated inductor can achieve similar, if not better, electrical performance (quality factor) above 10 MHz compared with the PCB design with approximately the same outer diameter, height, and inductance. In addition, the inductance and quality factor also match well with the simulation results shown in parentheses in Table I. About 10% discrepancy in quality factor may be introduced by the solder joints between the inductor and the SMA connected used for connecting to the network analyzer.

To demonstrate the mass reduction of our approach, two other inductor designs with similar dimensions (but different implementation schemes) were weighed for comparison: a 3.2-mm 1-oz copper PCB inductor in Fig. 2 and a T68-0 phenolic core. Note that the phenolic core is weighed alone, as there are different choices of wire size and type according to the intended application. However, the comparison is conservative, since adding copper windings to the core would increase the weight. The inductor nanofabrication approach

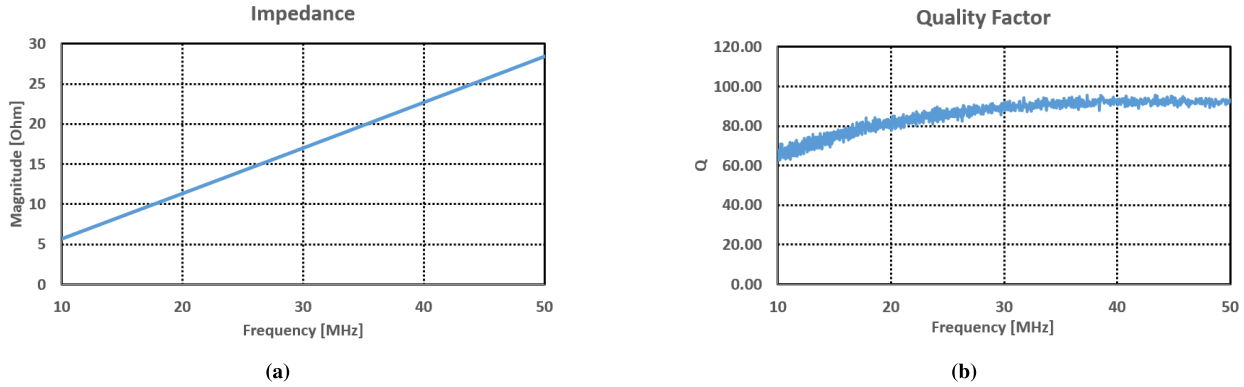

(a) (b)

Fig. 4. Impedance and quality factor versus frequency plots for inductor in Fig. 1(d). Measured by Agilent E5061B network analyzer. (a) Impedance magnitude versus frequency. (b) Quality factor versus frequency.

(a) (b) (c)

Fig. 5. Mass comparison of different air core inductor implementations. (a) Plated inductor weight reading is 0.71 g. (b) PCB inductor weight reading is 2.21 g. (c) T68-0 phenolic core weight reading is 1.6 g.

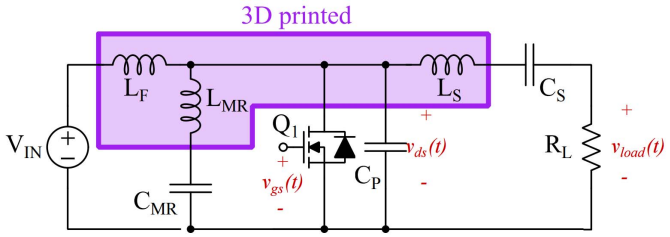

Fig. 6. Class Φ_2. Notice that L_F, L_{MR}, and L_S are sharing the same node.

of [13] for is not considered here as it would not be suitable for the targeted power and voltage level. The three parts and their masses are shown in Fig. 5(a)–(c). The pictures demonstrate the weight reductions achievable by the 3-D printing process. Further improvements in the design of the scaffolds will be explored (such as honeycomb fillings and sacrificial materials) to further reduce the weight of inductors.

III. Implementation and Experimental Verification

A. Class Φ_2 Inverter

To verify the performance of the proposed inductors, we designed a class Φ_2 inverter [11] as shown in Fig. 6, as it uses a single ground reference switch and small value resonant inductors. The class Φ_2 inverter of Fig. 6 can significantly reduce switch voltage stress by 30%–40% below that in class E-derived converters. Moreover, this type of switched mode resonant converter has been shown to operate efficiently at switching frequencies above 10 MHz. As described in the design procedure outlined in [11], four components (L_F, L_{MR}, C_{MR}, and C_P in Fig. 6) form a network of resonant passive components with an impedance tuned to shape the MOSFETs OFF-state voltage waveform to approximate a trapezoid with an amplitude of about 2 V_{IN}. The capacitor C_S connected in series with the load R_L blocks the dc component, while L_S determines the ac power to the load R_L. Detailed design guidelines and a description of the tuning procedure can be found in [11].

In this paper, to minimize issues in the 3-D inductor fabrication and relatively long time 3-D FEA simulation, as well as to simplify prototype implementation, we chose a design in which the three inductors L_F, L_{MR}, and L_S in Fig. 6 were of the same value. The implemented 90-nH inductor is shown in Fig. 1(d). Under this constraint, the electrical performance of the inverter is suboptimal, but was simple to implement using 3-D models and components that had been well characterized and studied throughout the course of this paper. With our choice of L_{MR} and following the design procedure in [11], we can find the value of the resonant capacitor C_{MR} using:

$$C_{MR} = \frac{1}{16\pi^2 f_s^2 L_{MR}} \tag{1}$$

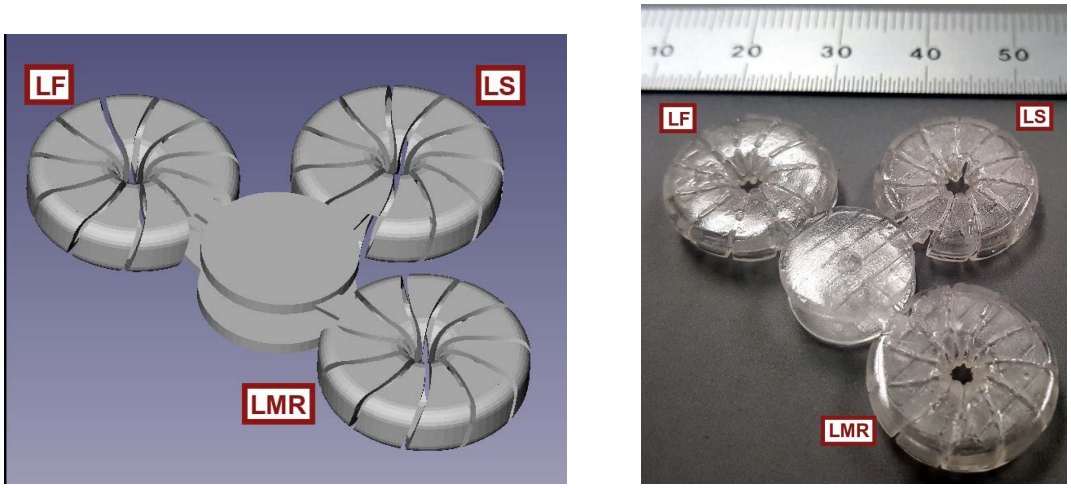

(a) (b)

Fig. 7. Single scaffold for the three inductors that share one node. (a) Initial print CAD model. (b) Scaffold was printed in Formlabs Form 2 and weighs 1.13g.

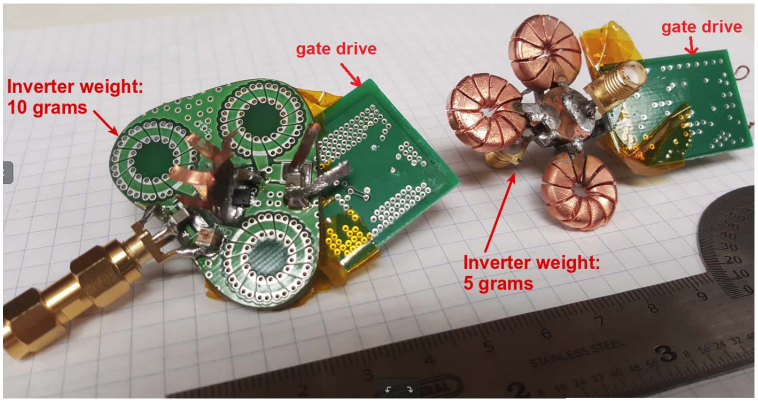

Fig. 8. Weight comparison of two inverters, 5 versus 10 g.

L_{MR} and C_{MR} are set to resonate at the second harmonic of the switching frequency (f_s) to achieve low impedance. The capacitor value of C_P is chosen to present a capacitive impedance at the third harmonic of the switching frequency with a magnitude that is several dBΩ lower than the impedance at the fundamental. Moreover, at a certain input voltage and output power, load resistance R_L can be calculated by [11, eq. (1)] as the L_S and R_L form a voltage divider in the output leg by selecting relatively large C_S.

In the Φ_2 inverter, the input inductor L_F plays an important role in setting the resonant characteristics of the network and usually carries a current with a large ac ripple. Also, the amplitude of the current in the resonant capacitor like C_{MR} can be quite high and may contain large harmonics components. Therefore, high-quality factors of both inductors and capacitors are desired to prevent penalty of overall efficiency as well as overheating.

B. Implementing Φ_2 Inverter With the 3-D Printed and Plated Scaffold

Moreover, one interesting feature of the Φ_2 inverter is that it has three resonant inductors sharing the same node as indicated in Fig. 6. Therefore, the three-inductor structure can be 3-D printed in a single 3-D scaffold, as shown in Fig. 7.

The center pads not only provide structural support for the floating 3-D printed structure, but also allow adequate drain/ground connection to the switching device. After plating, some sacrificial connections were cut to allow for the placement of the semiconductor and the capacitors of the design. The working inverter is shown on the right side of Fig. 8. Values of the components that form the inverter are listed in Table II.

TABLE II
PARAMETERS OF THE 14.2 MHz Φ_2 INVERTER

Parameter	Value
MOSFET	IPD530N15N3
L_F	90 nH
L_{MR}	90 nH
L_S	90 nH
C_P	520 pF
C_{MR}	330 pF
C_S	1 nF

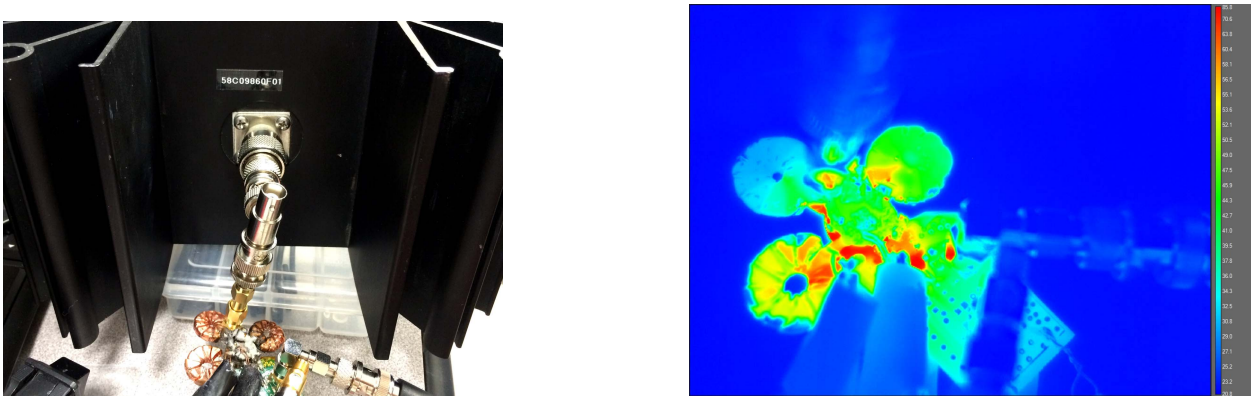

(a) **(b)**

Fig. 9. Inverter running on a 50-Ω load and thermal picture. (a) Inverter running on a 50-Ω RF load. (b) Thermal image of the inverter running with a 50-Ω load at 50 W full power. The maximum temperature point is about 80 °C at the gate driver chip.

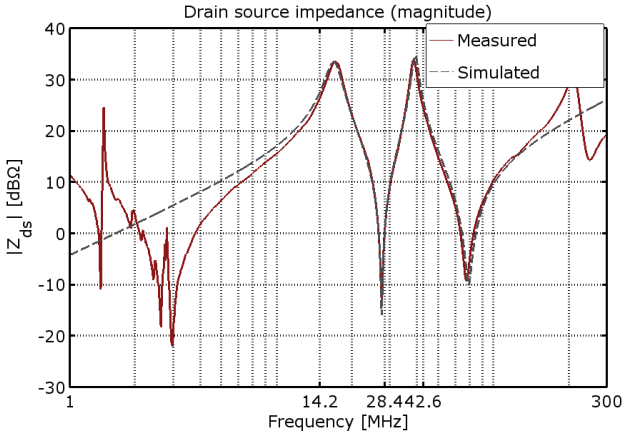

Fig. 10. Simulation versus measured drain to source impedance with resistive load.

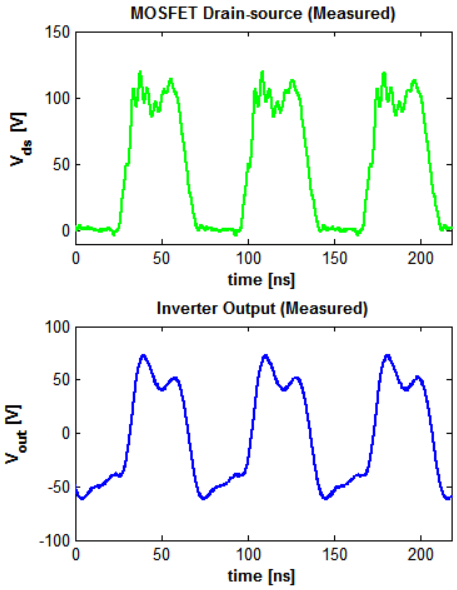

Fig. 11. Drain and output voltage with resistive load.

A 13.56-MHz 40-W Φ_2 inverter implemented with PCB inductors as described in [15] is also shown in Fig. 8 for weight comparison. A 50% reduction of the weight of the inverter (excluding the gate drive circuit and connectors) is achieved (5 versus 10 g). The gate drives in the two inverters in Fig. 8 use a single Texas Instruments LM5114 MOSFET driver IC and output a simple square voltage gating signal. The gate drive was implemented on a breakout PCB board to simplify prototyping. Weight reduction of the gate drive circuit is easily achievable by optimizing the layout (to minimize area) and using more specialized PCBs (to minimize thickness). Thus, the gate drive will not contribute greatly to overall weight. Further optimization could include the use of a semiconductor switch with integrated driver, potentially reaching a minimum in weight and size of the gate drive circuitry.

The inverter was first tested with a 50-Ω resistive load to verify the inductor design. Fig. 10 shows the comparison between the measured and the simulated MOSFET drain to source impedance. The good match at the frequencies interested indicates the components including inductors and MOSFET nonlinear capacitances are well modeled.

TABLE III
PERFORMANCE SUMMARY OF THE PROPOSED Φ_2 INVERTER

Parameter	Value
f_s	14.2MHz
V_{IN}	50V
P_{OUT}	50W
η	91%
Dimension	40 × 40 × 6 mm
Weight	5g (w/o connectors/gate drive)

Fig. 9(a) shows the test setup in which the inverter was connected to a 50-Ω RF load. Experimental drain and output voltage waveforms of the converter operating on a resistive load are shown in Fig. 11. The inverter delivers 50 W at a

Fig. 12. 3-D printed inverter with ICP running in a low-pressure argon ampoule.

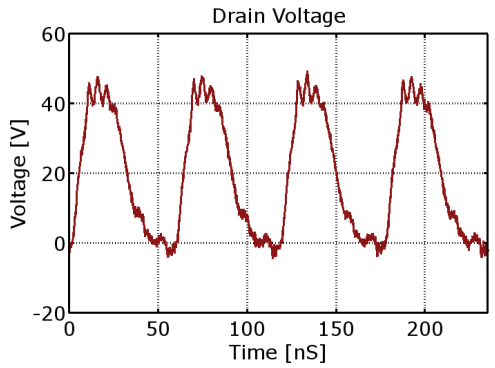

Fig. 13. Drain voltage with ICP.

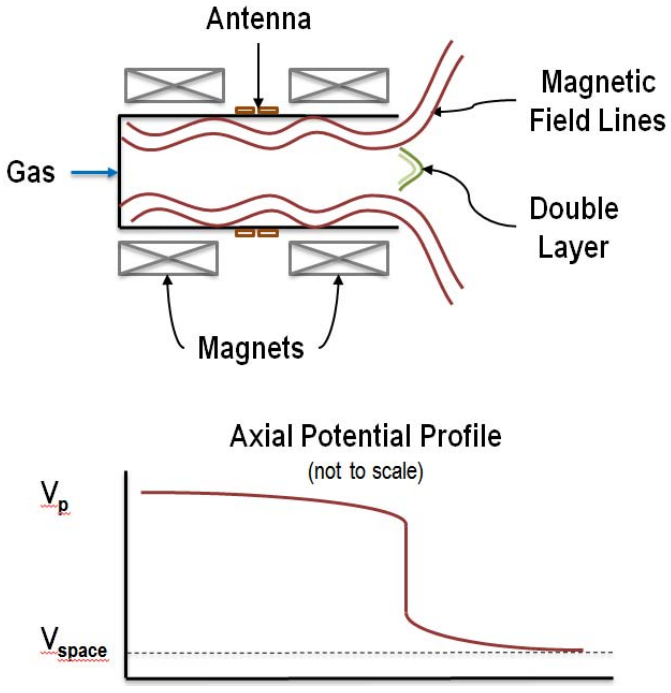

Fig. 14. HDL thruster schematics.

nominal input voltage of 50 V and achieves 91% efficiency. Further improvement of efficiency is expected by replacing the Si MOSFET with a state-of-the-art GaN FET. The thermal image shown in Fig. 9(b) was taken during the operation of

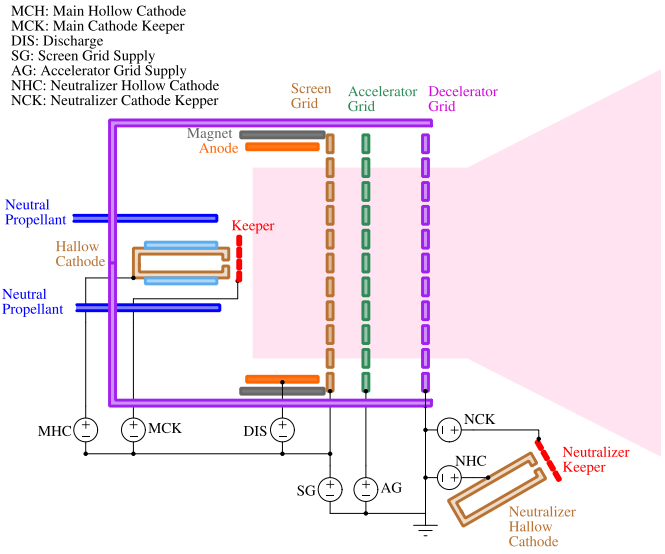

Fig. 15. Simplified schematic of an ion thruster. A conventional three-grid design needs seven powers supplies.

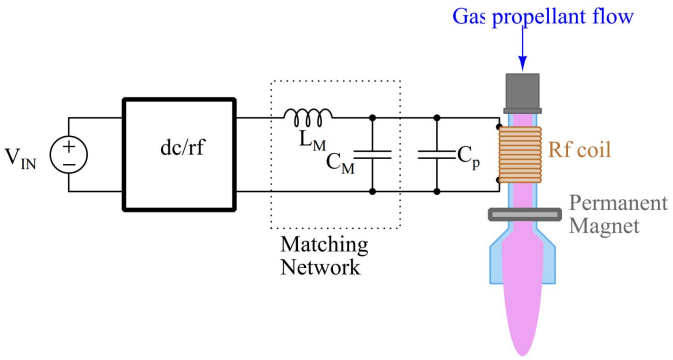

Fig. 16. Schematics of the plasma excitation coil.

full 50 W. The maximum temperature point is about 80 C at the gate drive IC. Table III summarized the proposed inverter performances.

IV. Driving an Inductively Coupled Plasma

To demonstrate the ability to drive a plasma load, the proposed power inverter was used to drive an ICP, which is an essential part of RF ion thrusters.

For convenience, initial testing of the converter driving the ICP was done in a low-pressure argon gas ampoule (a cylinder approximately 120 mm in length and 12 mm in diameter). The plasma RF coil consists of 16 turns of AWG 18 wire wound ($L_{\text{coil}} = 1.03\ \mu\text{H}$) upon the 12-mm argon ampoule. The RF coil was designed and characterized using an ENI A1000 RF power amplifier and large sinusoidal voltages. We swept the frequency of the amplifier to find the minimum power at which an ICP would strike with the coil. Approximately, 64 pF parallel capacitance C_P was added to the RF coil, yielding a network appearing resistive and having an impedance of approximately 200 Ω when driven with 52 W of RF power. The phase and impedance of this network vary with frequency and power delivery; to achieve an ICP requiring

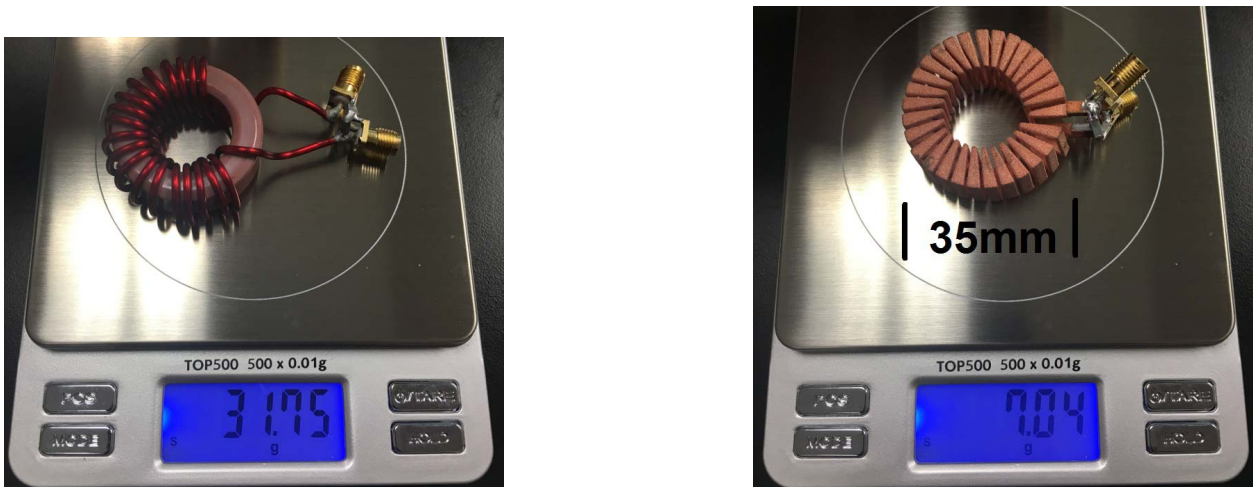

(a) (b)

Fig. 17. Matching network implementations. (a) Matching network with wire wound inductor (T130-0 core), weighing 31.75g. (b) Matching network with 3-D printed inductor, weighing 7.04g.

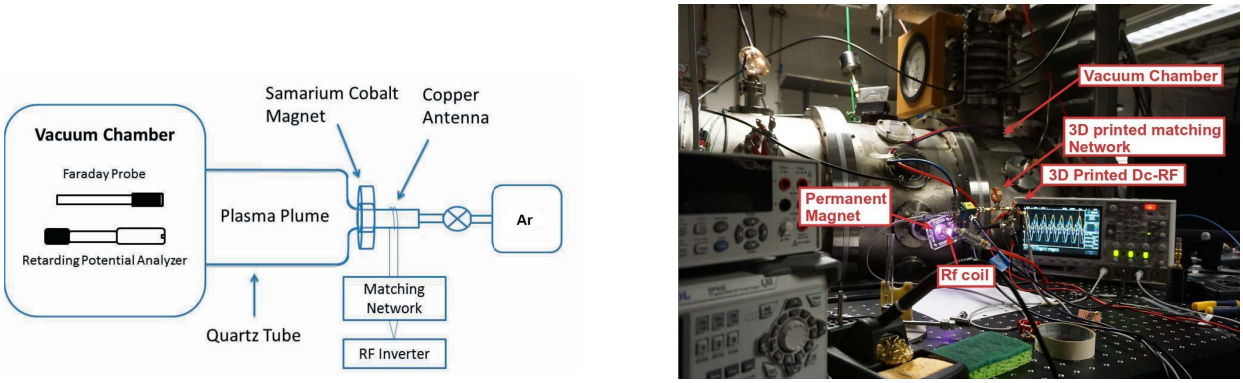

(a) (b)

Fig. 18. Vacuum testing environment setup. (a) Vacuum chamber setup schematics. (b) Vacuum chamber setup.

minimum power and possessing zero phase at the input of antenna network, a 105 V_{rms} sinusoid at 17.4 MHz was applied.

The 105 V_{rms} drive level and the resulted 200-Ω equivalent impedance are not conducive to the design of an inverter powered from a CubeSat's relatively low-voltage buses. Thus, a matching network was constructed to present a lower apparent impedance to the resonant inverter. A low-pass L matching network ($L_M = 694$ nH, $C_M = 134$ pF) was added in series with the RF coil.

The inverter in Fig. 9(a) was modified to operate at 17.4 MHz to drive the ICP in the argon ampoule. Fig. 12 shows the proposed inverter driving the ICP. Under this condition, the inverter draws 50 W peak power at an input of 20 V. Fig. 13 shows the measured drain node voltage waveform with the ICP load.

V. Driving a Helicon Double Layer Plasma

As an example application, the proposed inverter was tested as the power source for a HDL plasma thruster. In an HDL plasma thruster, plasma is formed by exciting a gas propellant using an RF coil. Thrust is created by the acceleration of positive ions from the plasma source due to the electric potential gradient generated by the current free electric double layer at the magnetic nozzle (e.g., dc magnetic coil or permanent magnets), as shown in Fig. 14.

The HDL plasma thruster is a promising step in the technological evolution of electric propulsion, as it has several advantages over other type of thrusters [6]–[8]. First, in an HDL plasma thruster, the ions are accelerated fast enough to eliminate the need for accelerating grids. Acceleration grid erosion is a lifetime-limiting process in ion thrusters, as is cathode and wall erosion in Hall thrusters. Second, as there is equal flux of electrons and positive ions from the HDL thruster, there is no need for an external neutralizer. Third, the absence of acceleration grids and external neutralizers leads to fewer power supplies required for HDL thruster than those of typical ion thrusters illustrated in Fig. 15. Fourth, HDL thrusters are able to run on a variety of propellants (such as water for high density fuel storage in [8]). Traditional electric propulsion options are limited to plasma propellants that do not react with the grids/electrodes (Xe, Ar, etc).

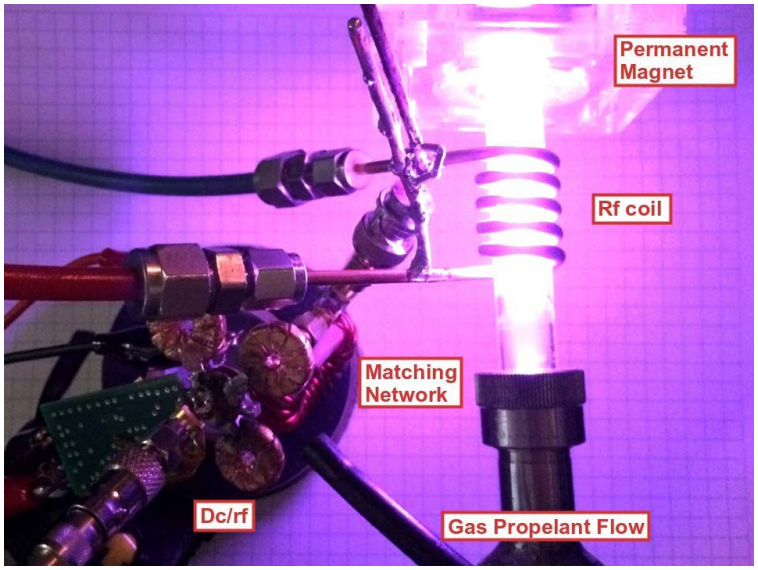

Fig. 19. Helicon running from 3-D printed inverter.

Vacuum experiments were conducted in the Stanford Plasma Physics Laboratory's small vacuum facility, with a custom quartz funnel (1 in. diameter) attached to a vacuum chamber on which the plasma coil (RF coil/antenna) was wound. The pressure in the chamber is pumped down to about 2×10^{-5} torr. Argon gas, at a flow rate of approximately 4 sccm, is used as the propellant and fed into the thruster. The dc magnetic field is created by the Samarium Cobalt permanent magnet, which has a flux density of several thousands of gauss.

The plasma coil was designed and characterized with HDL plasma load using an ENI A1000 RF power amplifier. A Pearson Model 6027 coaxial current monitor was used in conjunction with an ordinary voltage probe to determine the impedance magnitude and phase of the plasma load. Careful calibration and deskewing were performed on the voltage and current probe using a 50-Ω RF load before testing as the phase of probes or difference in cable lengths could compromise the phase measurement at tens of MHz. The finalized coil in the proposed design was made of a 5 turn wire wound solenoid ($L_{\text{coil}} = 180$ nH) copper wire. Subsequently, frequency was varied to find the optimal operation point to both initiate and sustain HDL. Approximately 700 pF parallel capacitance C_P was added to the antenna, yielding a network appearing resistive at 14.2 MHz and having an impedance of approximately 250 Ω when driven with 40 W of RF power.

Similarly, as in the previous ICP experiments, the RF voltage required to drive 250 Ω impedance at 40 W is too large for an inverter powered from a CubeSat's relatively low-voltage buses. Thus, a matching network was constructed to present a lower apparent impedance to the resonant inverter. A similar low-pass L matching network ($L_M = 830$ nH, $C_M = 130$ pF) as in the ICP testing matching the 250 Ω resistance from the load side to the 25 Ω resistance at source side was added in series with the antenna to yield the circuit of Fig. 16. Notice that C_P and C_M are in parallel and thus can be combined.

The matching network inductor was first implemented using a wire wound on a T-130 phenolic core and then evolved into the 3-D printed and plated air-core inductor, resulting in significant weight reduction (7.04 versus 31.75 g) for the matching network stage as shown in Fig. 17. The inductor in Fig. 17(b) was designed with a rectangular cross section for simplicity and quick iteration. And it is possible to further improve the inductor with the optimal cross section.

The combined matching network and plasma coil were characterized again using the A1000 RF power amplifier and calibrated voltage and current probes. Even though the matching network was designed to match a 25-Ω resistance on the source side, the measured impedance is around 50-Ω resistance due to the high nonlinearity of the plasma load. This impedance measurement motivated the inverter's testing with a 50-Ω resistive load; verification of performance on a resistive load is presented in Section III.

The complete experimental setup is shown in Fig. 18(a) and (b) after the A1000 RF power amplifier was replaced with the proposed inverter.

Fig. 19 shows the proposed inverter driving the HDL plasma. Fig. 20(a) and (b) shows the measured MOSFET drain voltage and plasma coil voltage waveforms. The current monitor was inserted between the matching network and the plasma coil to measure antenna current. The inverter was tested at an input voltage of 40 V, delivering 40 W at an overall efficiency (inverter and matching network) of 86%. Further optimization of the matching network inductor can be done to improve the overall efficiency. In addition to running the inverter at full 40 W, pulsed operation was also tested, as the power budget in a realistic CubeSat application will likely not achieve tens of watts but rather a few watts. The inverter was pulsed at 10% duty cycle at a rate of 10 kHz and was able to maintain the HDL plasma.

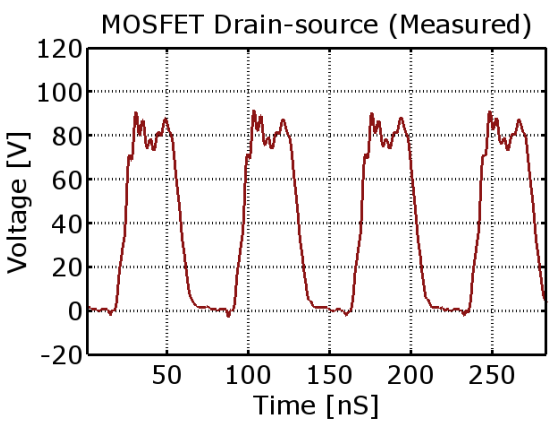

(a) MOSFET drain voltage with plasma load. The DC input voltage is 40V.

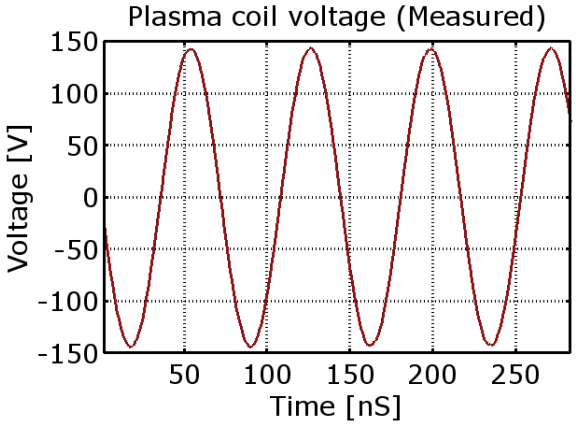

(b) Plasma coil voltage. V_{RMS} is about 102V.

Fig. 20. Measured drain and plasma coil voltage waveforms. (a) MOSFET drain voltage with plasma load. The dc input voltage is 40 V. (b) Plasma coil voltage. V_{rms} is about 102 V.

TABLE IV
EXPECTED PERFORMANCES OF OUR HDL THRUSTER

Parameter	Value
Thrust	1 mN
Specific Impulse	1500 s
Propellant	Water Vapor
Thrust Efficiency	15 %
Peak Power	40 W

For characterizing plasma properties, a similar measurement setup inside the vacuum chamber was used as in [8]. The expected performances of our HDL thruster are listed in Table IV. These specifications would allow a 10 kg CubeSat with dedicated 1U for propulsion, two-thirds of which would be propellant storage of 0.66 kg, to achieve an impulse of 1000 Ns in 145 days.

VI. CONCLUSION

This paper presents a 14.2-MHz 50-W resonant dc-RF power inverter implemented using 3-D printed and plated toroidal inductors with optimal cross sections. The weight of the proposed inverter is reduced by 50% compared with a 40-W state-of-the-art counterpart with all PCB printed inductors. The inverter achieves 90% efficiency when driving a resistive load. Furthermore, the inverter was able to successfully drive an ICP plasma and an HDL plasma thruster intended for CubeSat applications.

ACKNOWLEDGMENT

The authors would like to thank Prof. Sullivan at Dartmouth College for sharing the script used in [1].

REFERENCES

[1] C. R. Sullivan, W. Li, S. Prabhakaran, and S. Lu, "Design and fabrication of low-loss toroidal air-core inductors," in *Proc. IEEE Power Electron. Specialists Conf. (PESC)*, Jun. 2007, pp. 1754–1759.
[2] NASA. (2013). *Cubesats Released From Space Station*. [Online]. Available: http://www.nasa.gov/content/cubesats-released-from-space-station-0
[3] R. W. Conversano, D. M. Goebel, R. R. Hofer, T. S. Matlock, and R. E. Wirz, "Development and initial testing of a magnetically shielded miniature Hall thruster," *IEEE Trans. Plasma Sci.*, vol. 43, no. 1, pp. 103–117, Jan. 2015.
[4] J. J. Szabo *et al.*, "High throughput 600 watt Hall effect thruster for space exploration," in *Proc. 52nd AIAA/SAE/ASEE Joint Propuls. Conf.*, 2016, p. 4830.
[5] D. Kolosa, S. Spangelo, K. Lemmer, and J. Hudson, "Mission analysis for a micro RF ion thruster for CubeSat orbital maneuvers," in *Proc. Joint Propuls. Conf.*, Cleveland, OH, USA, 2014, pp. 1–13.
[6] F. F. Chen and R. W. Boswell, "Helicons—The past decade," *IEEE Trans. Plasma Sci.*, vol. 25, no. 6, pp. 1245–1257, Dec. 1997.
[7] C. Charles and R. Boswell, "Current-free double-layer formation in a high-density helicon discharge," *Appl. Phys. Lett.*, vol. 82, no. 9, p. 1356, 2003.
[8] D. Biggs *et al.*, "A compact helicon thruster for CubeSat applications," in *Proc. Joint Conf. 30th ISTS, 34th IEPC 6th NSAT*, Kobe, Japan, 2015, pp. 1–10.
[9] R. Boswell, C. Charles, P. Alexander, J. Dedrick, and K. Takahashi, "Plasma expansion from a radio frequency microdischarge," *IEEE Trans. Plasma Sci.*, vol. 39, no. 11, pp. 2512–2513, Nov. 2011.
[10] J. W. Kolar, J. Biela, S. Waffler, T. Friedli, and U. Badstuebner, "Performance trends and limitations of power electronic systems," in *Proc. 6th Int. Conf. Integr. Power Electron. Syst. (CIPS)*, Mar. 2010, pp. 1–20.
[11] J. M. Rivas, Y. Han, O. Leitermann, A. D. Sagneri, and D. J. Perreault, "A high-frequency resonant inverter topology with low-voltage stress," *IEEE Trans. Power Electron.*, vol. 23, no. 4, pp. 1759–1771, Jul. 2008.
[12] S. Orlandi *et al.*, "Optimization of shielded PCB air-core toroids for high-efficiency DC–DC converters," *IEEE Trans. Power Electron.*, vol. 26, no. 7, pp. 1837–1846, Jul. 2011.
[13] J. Kim, F. Herrault, X. Yu, M. Kim, R. H. Shafer, and M. G. Allen, "Microfabrication of air core power inductors with metal-encapsulated polymer vias," *J. Micromech. Microeng.*, vol. 23, no. 3, pp. 1–7, 2013.
[14] W. Liang, L. Raymond, and J. Rivas, "3-D-printed air-core inductors for high-frequency power converters," *IEEE Trans. Power Electron.*, vol. 31, no. 1, pp. 52–64, Jan. 2016.
[15] L. Raymond, W. Liang, J. Choi, and J. Rivas, "27.12 MHz large voltage gain resonant converter with low voltage stress," in *Proc. IEEE Energy Convers. Congr. Expo. (ECCE)*, Sep. 2013, pp. 1814–1821.

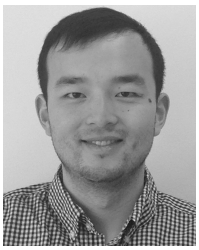

Wei Liang (S'12) received the B.Eng. degree from Northwestern Polytechnical University, Xi'an, China, and the M.S.E. degree from the University of Michigan, Ann Arbor, MI, USA, in 2011 and 2013, respectively. He is currently pursuing the Ph.D. degree with the Stanford University Power Electronics Research Laboratory, Stanford University, Stanford, CA, USA.

His current research interests include high frequency power electronics and the air-core passive components design for HF and VHF power conversion.

Luke Raymond (S'12) received the B.S.E. degree in mechanical engineering and the M.S.E degree in electrical engineering from the University of Michigan, Ann Arbor, MI, USA, in 2005 and 2012, respectively. He is currently pursuing the Ph.D. degree with the Stanford University Power Electronics Research Laboratory, Stanford University, Stanford, CA, USA.

He has industrial experience for seven years as a Consultant in the product development of mechanical and electrical systems. His current research interests include developing efficient high voltage power supplies for portable applications.

Max Praglin (S'15) received the B.S. degree in aeronautics & astronautics, and the M.S. degree in electrical engineering from Stanford University, Stanford, CA, USA, in 2015 and 2016, respectively.

He spent two years at the Stanford University Power Electronics Research Laboratory, Stanford University, focusing on HF and VHF resonant power converters. His current research interests include power electronics techniques that enable new applications, especially in aerospace, transportation, and telecommunication.

David Biggs was born in Omaha, Nebraska. He received the bachelor's degree of science in aerospace engineering from the University of Michigan, Ann Arbor, MI, USA, in 2012. Since 2012, he has been towardpursuing the Ph.D. degree with the Aeronautics and Astronautics Department, Stanford University, Stanford, CA, USA.

His current research interests include plasma physics with applications to microwave devices and photonics crystals, along with plasma propulsion.

Fabio Righetti received the B.S. degree in aerospace engineering from the University of Padova, Padua, Italy, in 2011, and the M.S. degree in aeronautical engineering from the Politecnico di Milano, Milan, Italy, in 2014. He is currently pursuing the Ph.D. degree with Stanford University, Stanford, CA, USA.

His current research interests include plasma propulsion for space applications, high energy plasma accelerators, and plasma photonic crystals.

Mark Cappelli received the B.A.Sc. degree in physics from McGill University, Montréal, QC, Canada, in 1980, and the M.A.Sc. and Ph.D. degrees in aerospace science and engineering from the University of Toronto, Toronto, ON, Canada, in 1983 and 1987, respectively.

He is currently a Professor with the Department of Mechanical Engineering, Stanford University, Stanford, CA, USA. His current research interests include broad aspects of plasmas and gas discharges as they apply to aerodynamic and space propulsion, combustion, electromagnetics, and material processing.

Brian Holman received the bachelor's degree and the B.S. degree in mechanical engineering from Stanford University, Stanford, CA, USA, where he is currently pursuing the master's degree in electrical engineering.

He specializes in using his combined background to design packaging and cooling solutions for power electronic devices.

Juan Rivas Davila (S'01–M'06) was born in Mexico, Mexico. He received the B.A.Sc. degree from the Monterrey Institute of Technology, Monterrey, Mexico, in 1998, and the S.M. and Sc.D. degrees from the Laboratory of Electromagnetic and Electronic Systems, Massachusetts Institute of Technology, Cambridge, MA, USA, in 2003 and 2006, respectively.

From 2007 to 2011, he was a Power Electronics Engineer with the High-Frequency Power Electronics Group at the General Electric Global Research Center, Niskayuna, NY, USA. From 2011 to 2013, he was an Assistant Professor at the University of Michigan, Ann Arbor, MI, USA. In 2014, he joined the Electrical Engineering Department, Stanford University, Stanford, CA, USA, as an Assistant Professor. His current research interests include power electronics, RF power amplifiers, resonant converters, soft switching topologies, and the design of air-core passive components for VHF power conversion.